Supplementary Figure 1. Zhou et al., 2019

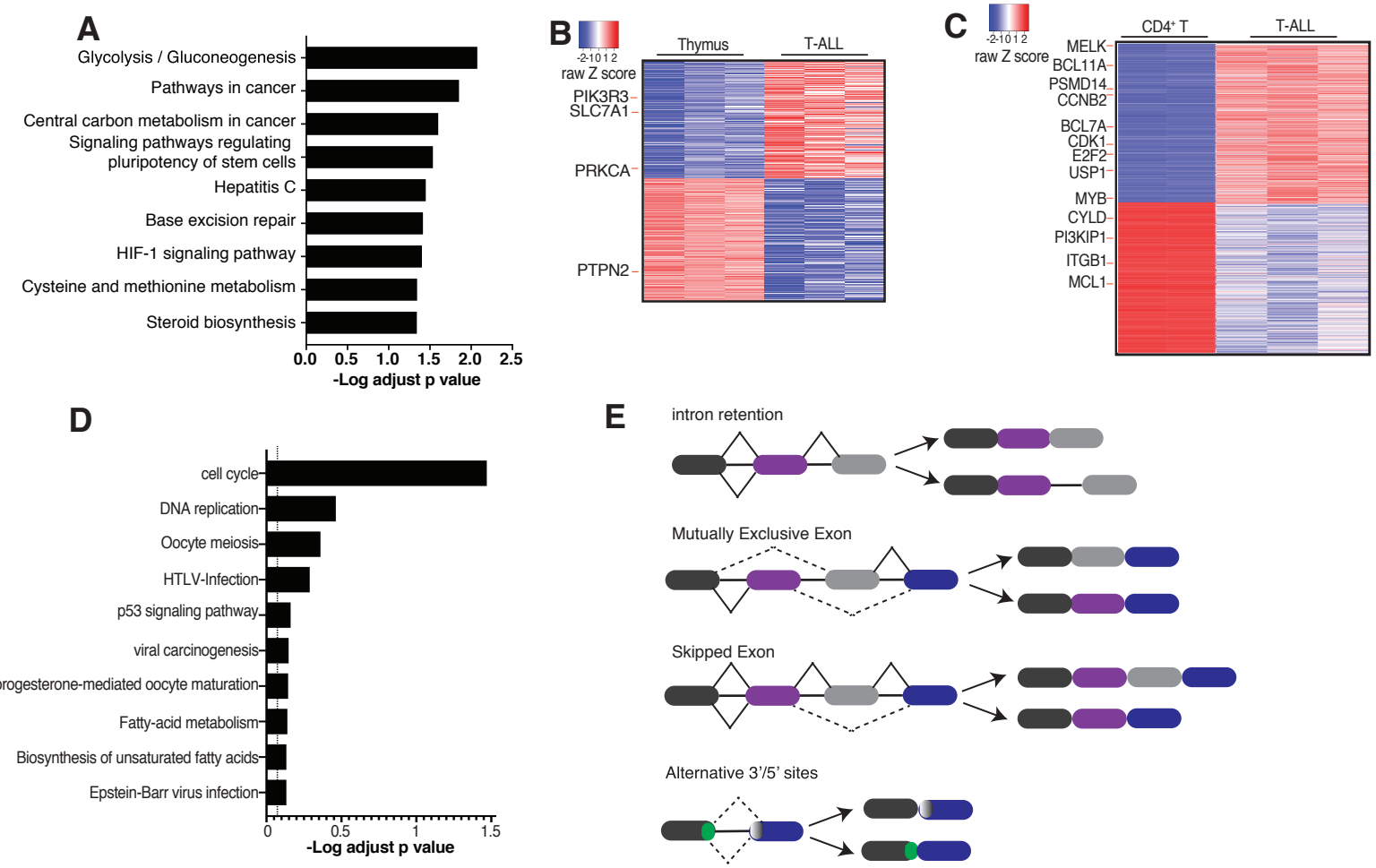

Supplementary Fig. 1. Gene expression changes in T-ALL compared to normal T cell subtypes. A, Kyoto Encyclopedia of Genes and Genomes (KEGG) analysis for differentially expressed genes in T-ALL compared to $CD3^+$ T cells. **B,** Heatmap of changes in expression of the 406 most significantly up-regulated genes and 426 down-regulated genes in three T-ALL patient samples compared to thymocytes, ranked based on gene expression levels in T-ALL (n=3, adj. $P<0.01$). **C,** Heatmap of changes in expression of the 421 most significantly up-regulated genes and 399 most significantly down-regulated genes in T-ALL patient samples compared to $CD4^+$ T cells, ranked based on gene expression levels in T-ALL ($n=3$, adj. $P<0.01$). **D,** KEGG analysis for differentially expressed genes in T-ALL compared to $CD4^+$ T cells. **E,** Schematic representation of the different types of splicing.

Supplementary Figure 2. Zhou et al., 2019

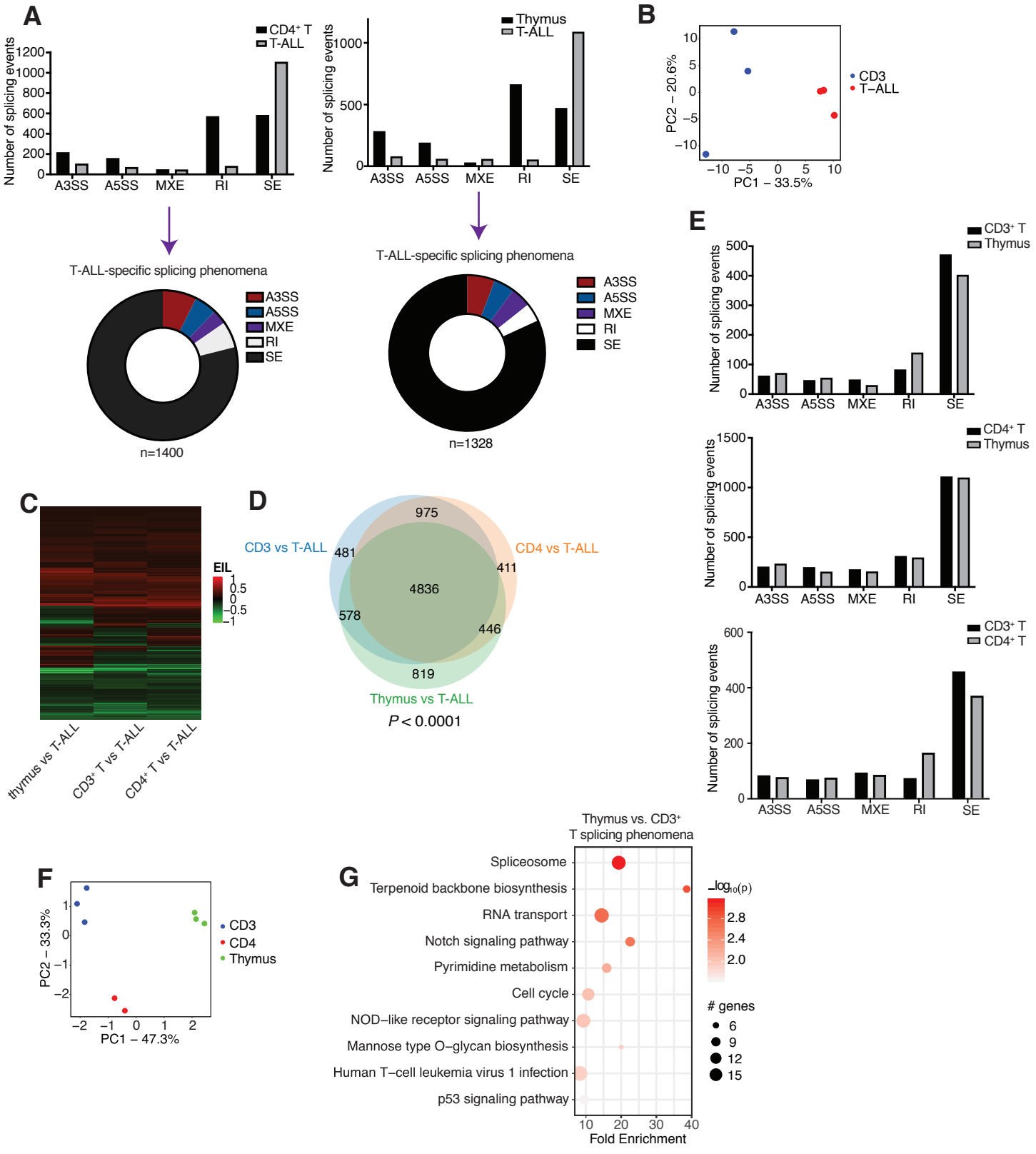

Supplementary Fig. 2. Extensive alterations in exon skipping events in T-ALL compared to normal T cell subtypes. A, Number of splicing events in T-ALL cells versus $CD4^+$ T cells (left side) and thymocytes (right side). Bar graphs (top) represent different types of splicing events, and pie charts (bottom) correspond to the grey bar from the bar-graph and indicate T-ALL-specific splicing phenomena. The plot represents the MATS analysis using three biological replicates per group. Events with PSI>0.1 are presented (FDR<0.05). Retained introns (RI) and skipped exons (SE) were the two event categories affected most dramatically. A3SS, alternative 3' splice sites; A5SS, alternative 5' splice sites; MXE, mutually exclusive exons. **B,** Principal component analysis (PCA) of skipped exon events for $CD3^+$ T cells and T-ALL patients. **C,** Heatmap of differential exon inclusion in T-cell subtypes compared to T-ALL, as quantified via exon inclusion levels (EIL). Positive (red) values represent exon inclusion events whereas negative (green) values represent exon exclusion events in the thymus, $CD3^+$ and $CD4^+$ T cells compared to T-ALL. Panels **A** and **C** collectively show that there are more skipped exons in T-ALL compared to normal T cells. **D,** Overlap of differentially spliced transcripts in $CD3^+$ T cells, $CD4^+$ T cells and thymocytes compared to T-ALL (*PSI*> 0.05, FDR<0.05). This panel suggests that T cell populations have a splicing landscape significantly distinct from T-ALL, irrespective of their differentiation status. **E,** Number of splicing events in the different T cell subtypes. Bar graphs represent different types of splicing in $CD3^+$ T cells vs. thymocytes (top panel), $CD4^+$ T cells vs. thymocytes (middle panel) and $CD3^+$ vs. $CD4^+$ T cells (lower panel). Skipped exons (SE) were the main event category affected. **F,** Principal component analysis (PCA) of skipped exon events comparing three different cell types, $CD3^+$, $CD4^+$ T cells and thymocytes. **G,** Kyoto Encyclopedia of Genes and Genomes (KEGG) analysis showing main transcript families enriched in splicing events in thymocytes compared to $CD3^+$ T cells. Transcript categories are ranked based on the enrichment, *P* value and size of the group.

Supplementary Figure 3. Zhou et al., 2019

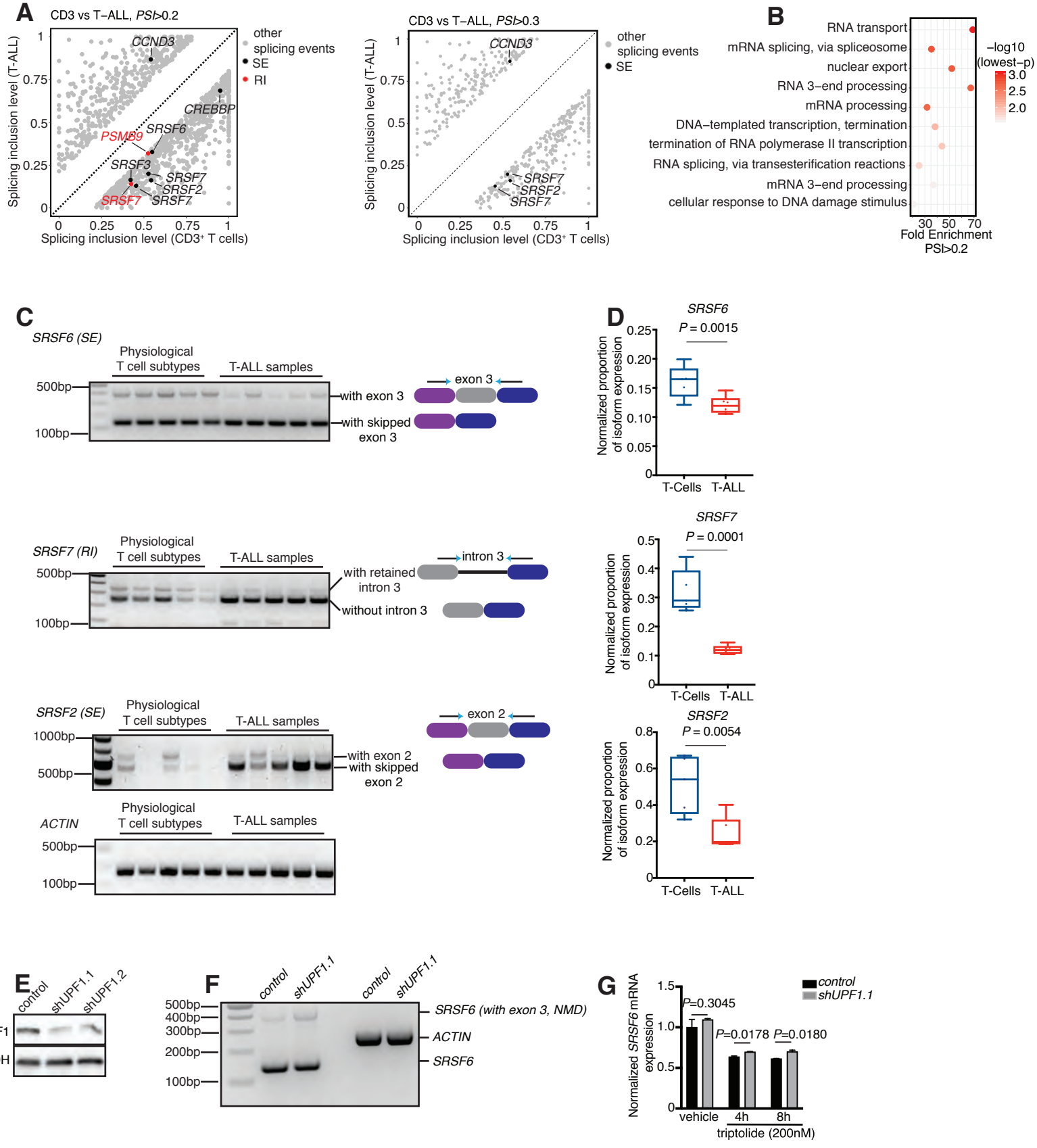

Supplementary Fig. 3. SRSF transcripts present with splicing alterations in T-ALL compared to physiological T cells. A, Scatterplots of splicing changes and distribution in T-ALL compared to $CD3^+$ T cells. Selected transcripts are colored based on the type of differentially spliced event. Splicing is quantified using rMATS and transcripts presenting *PSI*>0.2 (left panel) and PSI>0.3 (right panel) of transcripts are shown. **B,** Gene ontology analysis showing main transcript families enriched in splicing events in T-ALL compared to $CD3^+$ T cells (*PSI*>0.2). Transcript categories are ranked based on the enrichment, *P* value and size of the group. **C,** PCR reactions for splicing event confirmation in T-ALL compared to T cells. **D,** Quantification of band intensities from panel **C**. **E,** Immunoblot for UPF1 levels upon silencing of the transcript using short hairpin against *UPF1* (*shUPF1.1* and *shUPF1.2*) in JURKAT cells. **F, G,** Detection and quantification of the NMD-related, exon-3 containing, isoform of SRSF6 in T-ALL: One representative DNA gel from the end-point PCR study of *shUPF1.1*- or control(*shcontrol*)-expressing JURKAT cells (**F**) as well as real-time quantitative PCR from three replicates post treatment of *shUPF1.1*- or control (*shcontrol*)-expressing JURKAT cells with 200nM Triptolide transcriptional inhibitor for 4h and 8h (**G**) are shown.

Supplementary Figure 4. Zhou et al., 2019

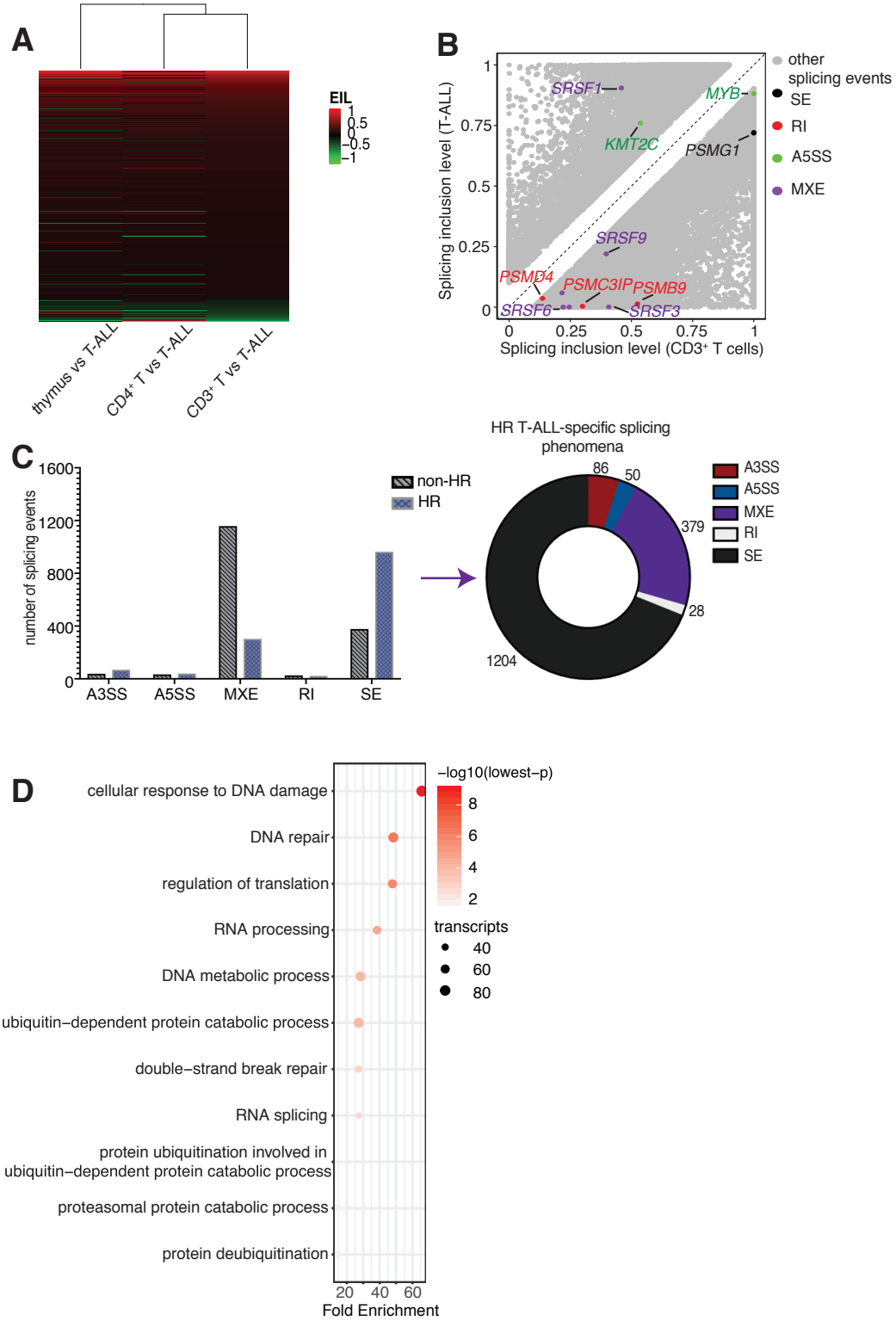

Supplementary Fig. 4. High-risk T-ALL presents with a splicing landscape different than standard-risk T-ALL. A, Heatmap of differential exon inclusion in T-cell subtypes compared to the validation cohort of T-ALL (*n*=14), as expressed via exon inclusion levels (EIL). Positive (red) values represent exon inclusion events whereas negative (green) values represent exon exclusion events in the thymus, $CD3^+$ and $CD4^+$ T cells compared to T-ALL. **B,** Scatterplot analysis representing the type and distribution of splicing changes in the T-ALL validation cohort (*n*=14) compared to $CD3^+$ T cells (*FDR* < 0.05; *PSI* > 0.1). Selected transcripts belonging to epigenetic modulators (i.e. *KMT2C*), oncogenes (i.e. *MYB)* and the proteasome (i.e. *PSMG1*) and associated splicing categories are shown. **C,** Comparison of splicing events in HR and non-HR T-ALL patient samples in the validation cohort. Bar graph (left) compares HR and non-HR events and pie chart (right) shows the number of HR-specific splicing phenomena. **D,** Gene ontology analysis for differentially spliced transcripts in HR compared to non-HR T-ALL cells.

Supplementary Figure 5. Zhou et al., 2019

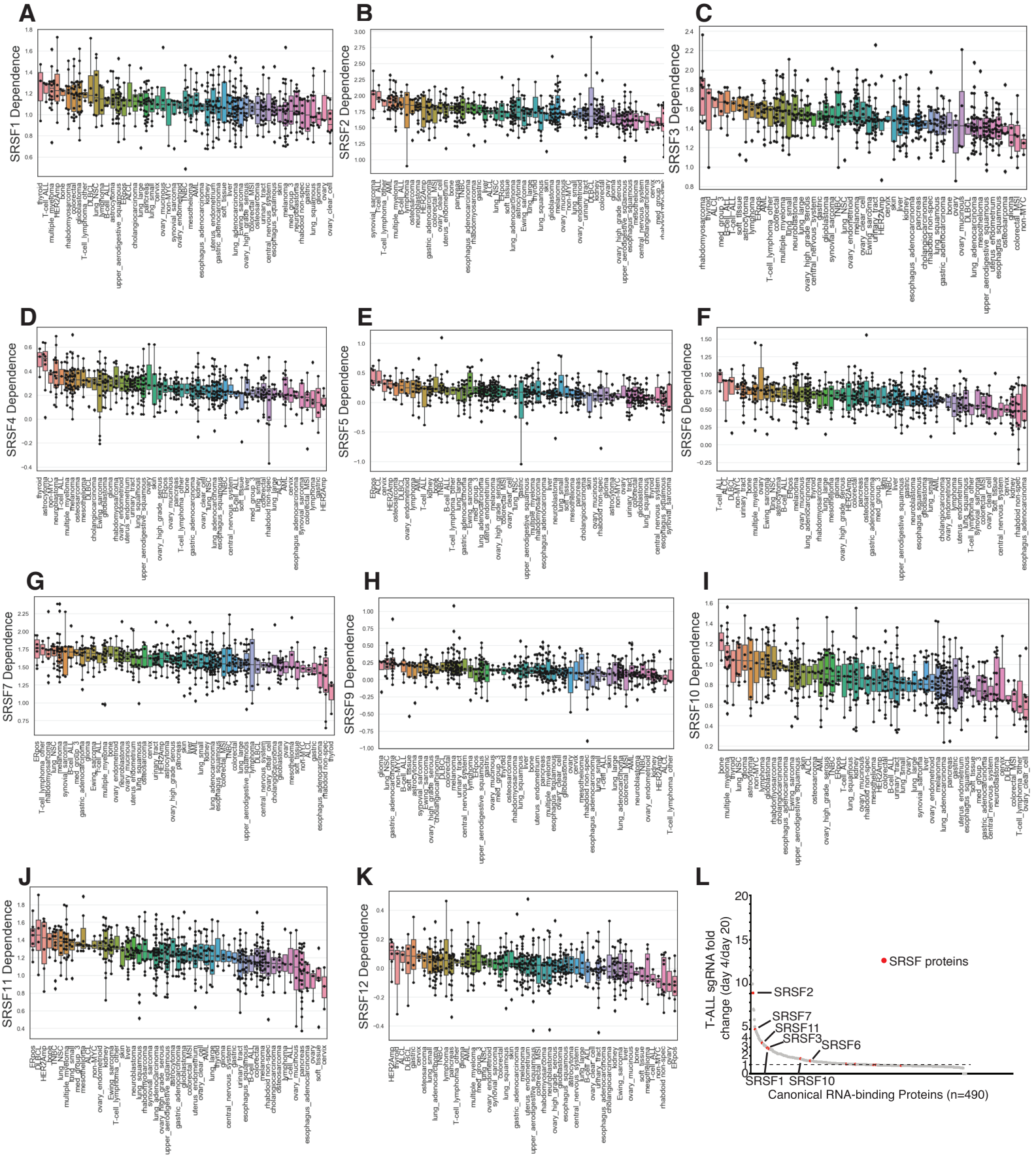

Supplementary Fig. 5. Essentiality for all *SRSF* genes in cancer. A-K, Essentiality for SRSF transcripts amongst different cancer types from the Project *Achilles*. A gene essentiality score of 1 is typical for genes considered pan-essential, such as ribosome components. T-ALL and other representative cancer types are shown. B-ALL, B cell acute lymphoblastic leukemia; TNBC, triple-negative breast cancer; AML, acute myeloid leukemia. **L,** Fold change (day 4/day 20) in *sgRNA* abundance assessed by high-throughput sequencing in the pooled RBP-focused negative selection screen in JURKAT T-ALL cells. Each dot represents the average abundance of all sgRNAs targeting an RBP and dots representing depleted *SRSF* transcripts (red) are labeled.

Supplementary Figure 6. Zhou et al., 2019

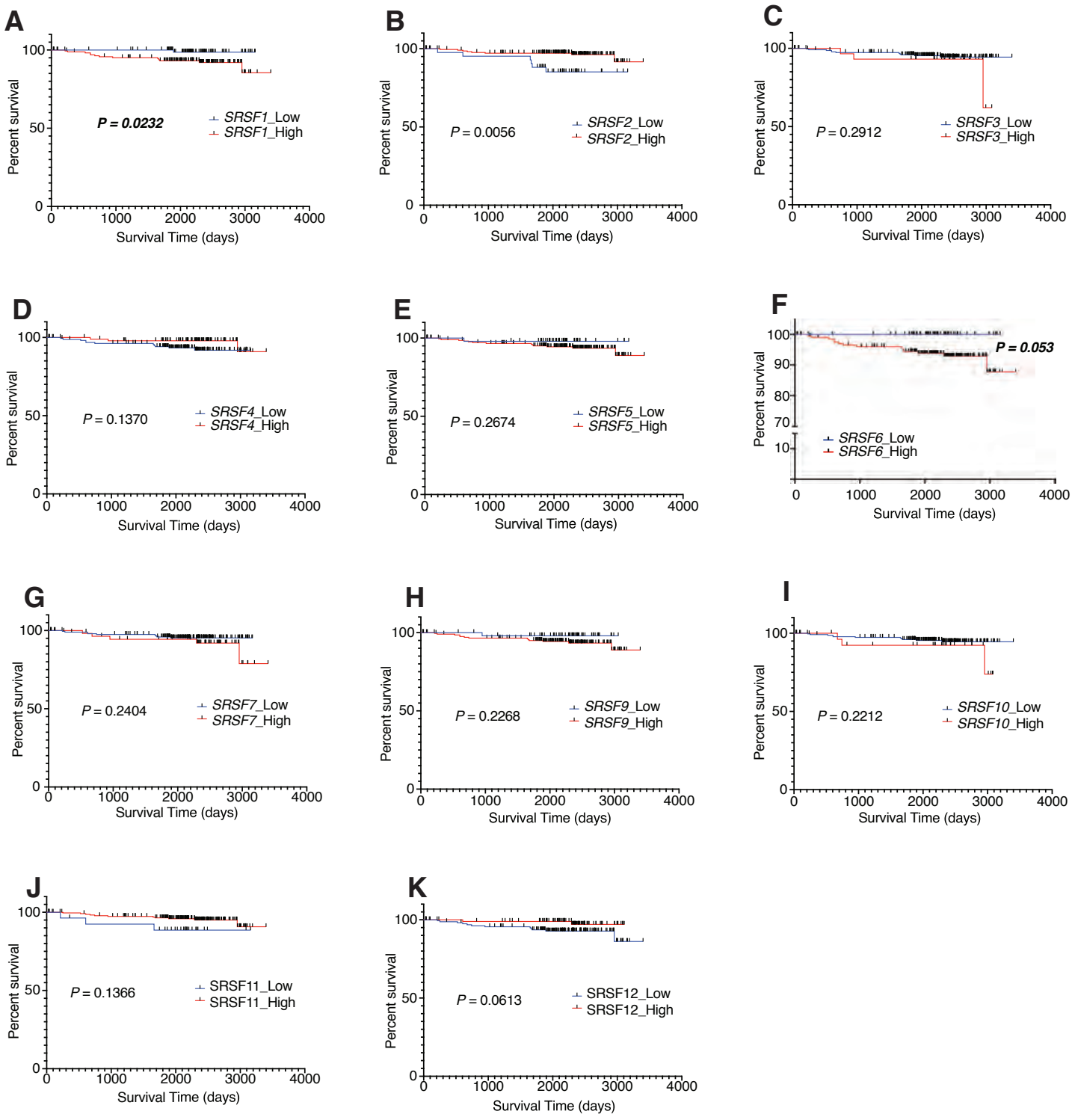

Supplementary Fig. 6. Survival curves (A-K) from pediatric T-ALL patients (the Pediatric Cancer Genome Project) clustered based on high or low *SRSF* mRNA levels. Note that SRSF6 is expressed at very low levels in T-ALL and was excluded from the study.

Supplementary Figure 7. Zhou et al., 2019

A

Gene	Mutations	Samples	Missense	Frameshift	Protein insertion	Nonsense	Protein deletion	Splice region	Splice
NOTCH1	264	196	140	47	32	22	23		
SF3B1	2	2	2						
SF3B2	1	1						1	
U2AF1	4	4	4						

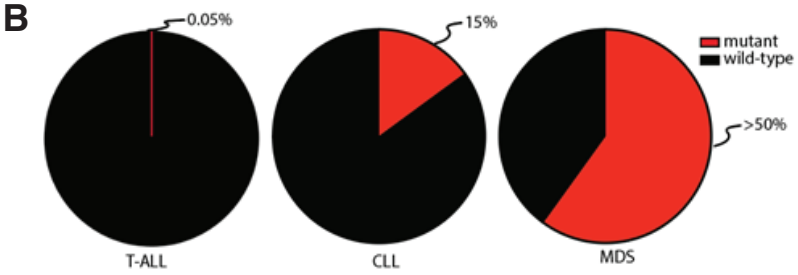

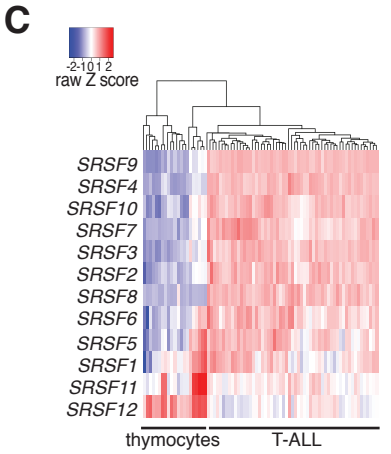

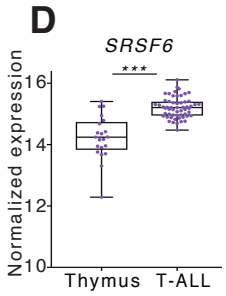

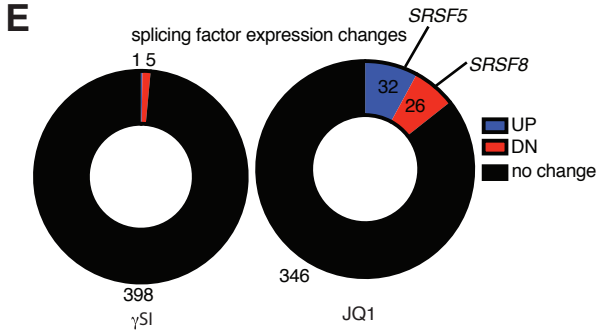

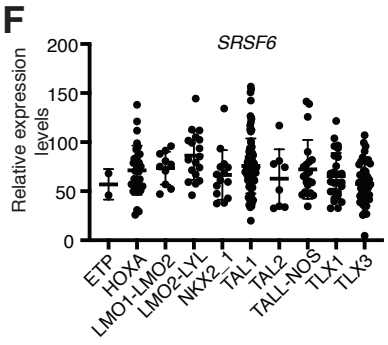

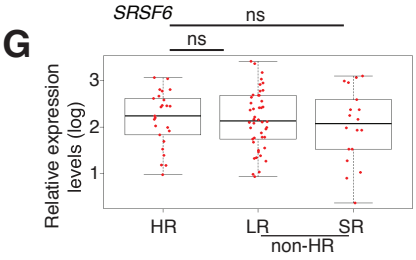

Supplementary Fig. 7. T-ALL is characterized by very few genetic alterations in the splicing genes. A, Analysis of mutations in splicing factors in T-ALL (data from the Pediatric Cancer Genome Project). **B,** A comparison of mutational status in T-ALL, chronic lymphocytic leukemia (CLL) and myelodysplastic syndromes (MDS). **C,** Heatmap of gene expression changes in *SRSF* transcripts in T-ALL versus thymocytes. 57 T-ALL patient samples and 21 thymocytes were used in this comparison. **D,** *SRSF6* mRNA expression in T-ALL versus thymocytes (samples from c were used). **E,** Gene expression changes for splicing factor transcripts in the presence of gamma secretase inhibitor (γSI), which inhibits NOTCH1, or JQ1, a bromodomain inhibitor that inhibits MYC. **F, G,** *SRSF6* mRNA expression levels in different T-ALL subtypes (**F**) and HR vs non-HR (Low- (LR) and standard-risk (SR)) T-ALL (**G**). *ns*, non-significant.

Supplementary Figure 8. Zhou et al., 2019

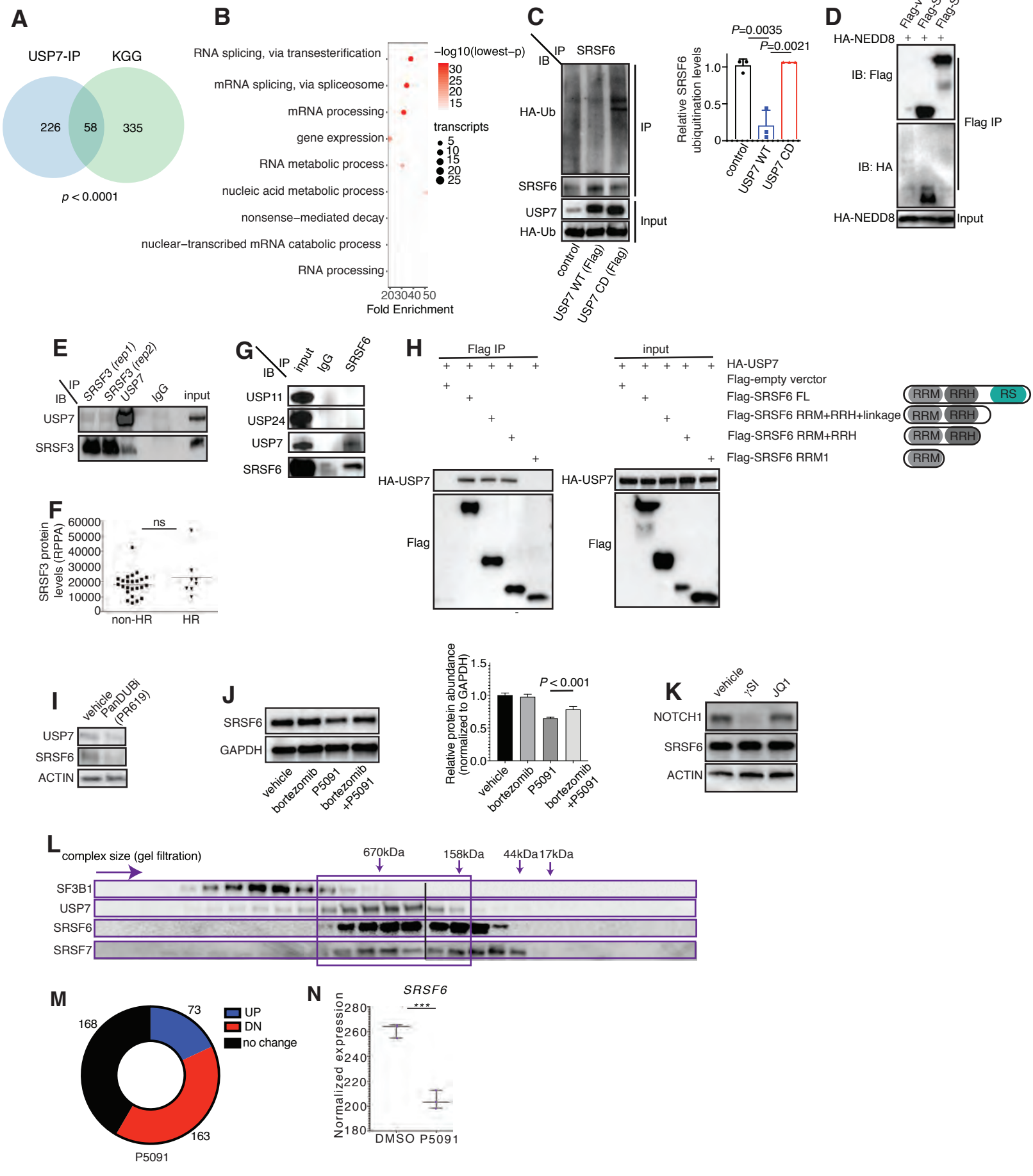

Supplementary Fig. 8. SRSF6 is regulated at the posttranslational level in T-ALL. A, Overlap of mass spectrometry data upon USP7 immunoprecipitation and KGG mass spectrometry. Shown is the overlap of peptides belonging to 58 proteins. **B,** Gene ontology analysis showing main protein families represented by the 58 proteins (from **A**). **C,** Immunoblot for detection of ubiquitination upon lentiviral expression of SRSF6 together with HA-ubiquitin and Flag-tagged wild-type or catalytically deficient (CD) USP7 in 293T cells (left panel). HA antibody incubated membrane for ubiquitin detection upon pull down of SRSF6 using SRSF6 antibody. A representative blot for one biological replicate for the pull-down and immunoblot studies is shown. Right panel shows quantification of SRSF6 poly-ubiquitination levels in control, USP7 WT and USP7 CD conditions relative to SRSF6 protein levels and then relative to the polyubiquitination signal in the USP7 CD condition that was set as 1 (*n=3*). **D,** Immunoblot for neddylation assay coupled to HA immune-precipitation in 293T cells. Flag-tagged SRSF6 and SRSF3 (positive control) were expressed in 293T cells together with HA-Nedd8 protein for detections of neddylation. **E,** Immunoblot studies following immunoprecipitation (IP) of SRSF3 in two replicates and USP7 in JURKAT T-ALL cells, showing interactions of SRSF3 with USP7. **F,** RPPA analysis for SRSF3 protein levels in HR (n=8) vs. non-HR T-ALL (n=24) cases. **G,** Immunoblot studies following immunoprecipitation (IP) of SRSF6 in CUTLL1 T-ALL cells, showed no interaction of SRSF6 with USP11 and USP24. **H,** Immunoblot studies following transfection of 293T cells with HA-tagged USP7 as well as full-length and truncated versions of Flag-tagged SRSF6 and immunoprecipitation (IP) using antibodies against the Flag epitope. The results suggest that the RRH domain of SRSF6 is critical for the interaction with USP7. RS: serine/arginine (S/R)-rich domain; RRM: RNA recognition motif, RRH: RRM homology. **I** USP7 and SRSF6 protein expression changes upon treatment of JURKAT cells with pan-deubiquitinase inhibitor PR-619 (10 μm) for 24 h. **J,** SRSF6 protein levels upon treatment of JURKAT cells with P5091, bortezomib or their combination over a period of 24h. Immunoblot (left panel) and quantification of protein levels using three replicate experiments (right panel) are shown. **K,** SRSF6 protein expression changes upon treatment of JURKAT cells with γSI (2.5μM), JQ1 (300nM), or P5091 (10μM) for 24 h. NOTCH1 is used as a control for the γSI treatment. **L,** Immunoblot studies for SF3B1, USP7, SRSF6, and the SRSF6-interacting protein SRSF7 following isolation of whole-cell extracts and size exclusion chromatography. Fractions containing high to low molecular weight complexes (left to right) were run on a gradient 4-15% polyacrylamide gel. For all immunoblots presented here, 1 of 3 representative biological replicates is shown. **M, N,** Expression changes (RNA-seq) for splicing factor genes (**M**) and SRSF6 mRNA (**N**) upon USP7 inhibition using 10μM P5091 (24h).

Supplementary Figure 9. Zhou et al., 2019

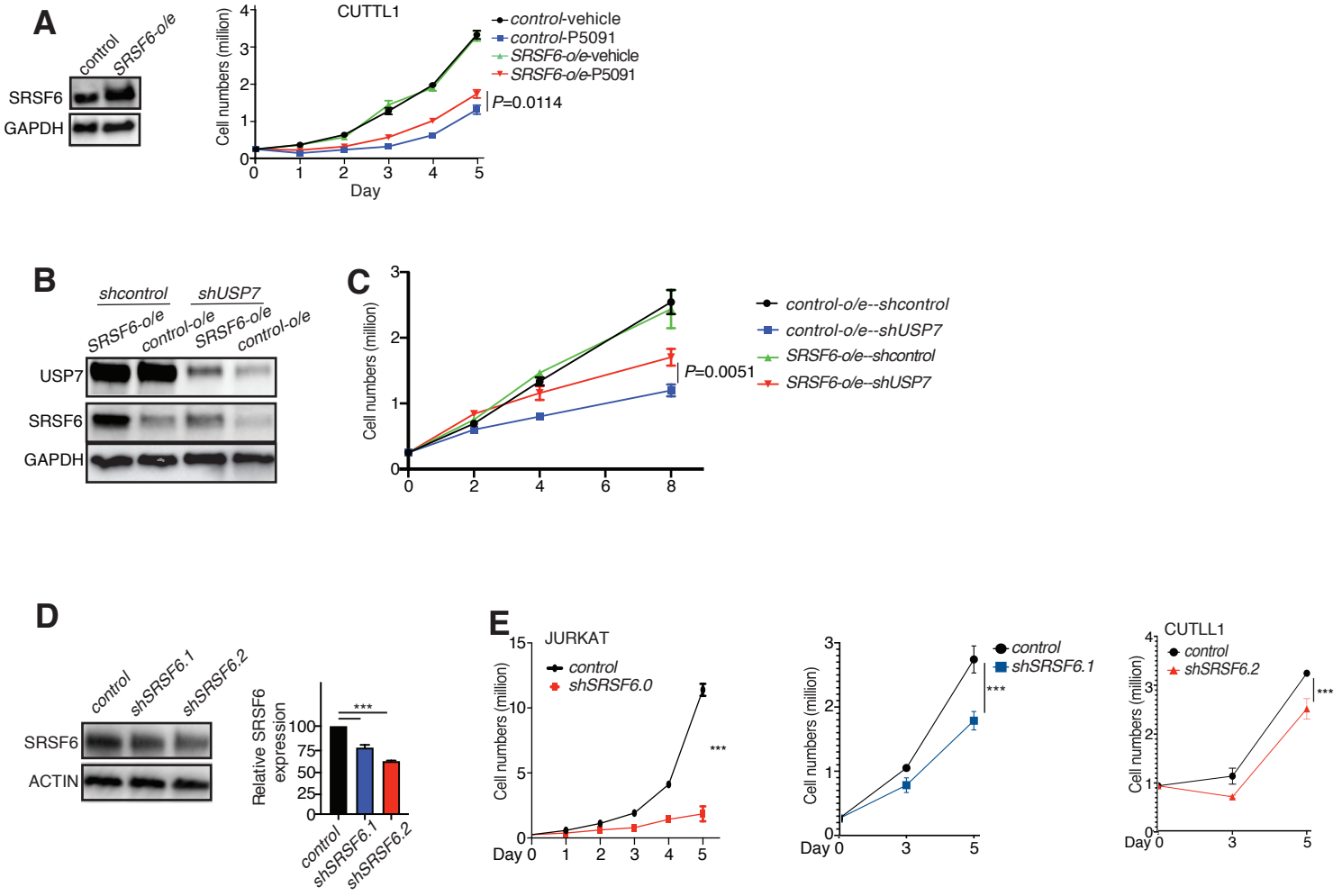

Supplementary Fig. 9. SRSF6 is a critical factor for leukemia growth. A, Overexpression of flag-tagged SRSF6 in CUTLL1 cells. Immunoblot for the expression of SRSF6 (left panel) and growth of control and *SRSF6-o/e* CUTLL1 cells over a period of 5 days (right panel) are presented (n=3). **B, C,** Overexpression of SRSF6 in CUTLL1 cells followed by inducible silencing of USP7. One of three representative immunoblots for the expression of SRSF6 and USP7 (**B**) and growth of control and *SRSF6-o/e* CUTLL1 cells over a period of 8 days from the initiation of USP7 silencing are shown (**C**, n=3). GAPDH is used as a loading control in the immunoblot study. **D,** Immunoblot analysis (left) and quantification (right) of SRSF6 protein levels (n=3) in JURKAT cells expressing control hairpin RNA as well as two hairpin RNAs against *SRSF6* (control, *shSRSF6.1* and *6.2* n=3, *** P<0.001). ACTIN is used as loading control. **E,** Cell growth of control (*scramble, left panel*) and *shSRSF6.0*- (middle panel), *shSRSF6.1*- (right panel, JURKAT) or *shSRSF6.2*-expressing (CUTLL1) cells over a period of 5 days post puromycin selection (n=3, ***, P<0.001).

Supplementary Figure 10. Zhou et al., 2019

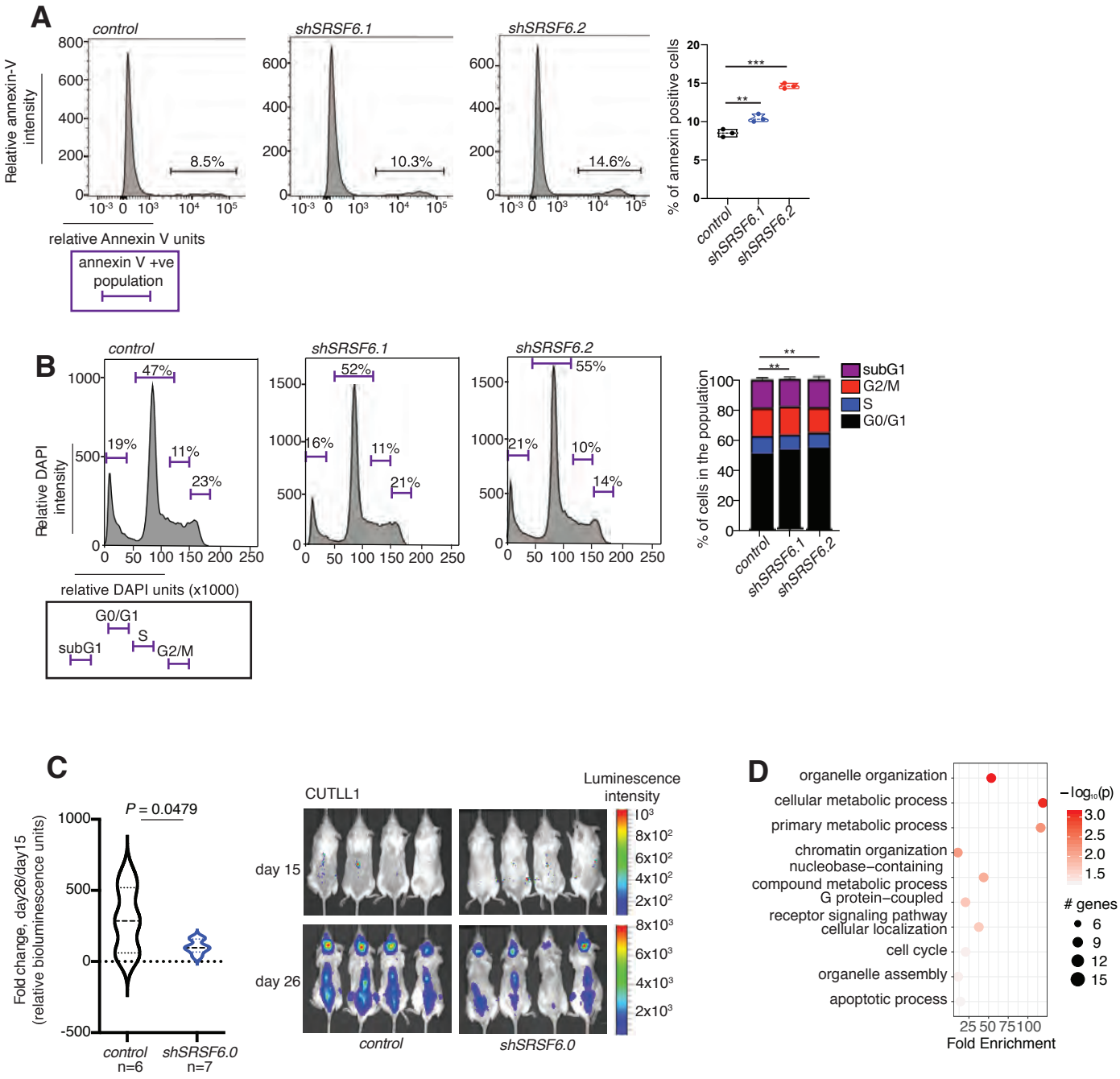

Supplementary Fig. 10. SRSF6 silencing alters apoptosis and cell cycle of leukemia cells. A, Annexin V staining for control (*PLKO.1*), *shSRSF6.1*- and *shSRSF6.2*-expressing CUTLL1 cells 72 h post-puromycin selection. Representative plots depicting annexin V level assessed via flow-cytometry (first three panels) and quantification (right panel) from three biological replicates are shown. (n=3, **, P<0.01; ***, P<0.001). **B,** Cell cycle analysis using DAPI staining for 3 h coupled to flow cytometry, for *control*, *shSRSF6.1*- and *shSRSF6.2*-expressing CUTLL1 (first three panels), and quantification (right panel) from three biological replicates, 72 h post-puromycin selection. (n=3; **, P<0.01). **C,** Luciferase-expressing CUTLL1 cells were transduced with lentiviral vector expressing a control hairpin RNA or *shSRSF6.0*, selected using puromycin for a period of 11 days, and injected intravenously into immunocompromised mice. Leukemic burden was assessed via blast detection in mouse body using bioluminescence and IVIS equipment twice per week. Relative bioluminescence intensity is shown for four representative mouse per treatment group on days 15 and 26 of treatment (left panel). The fold change in total flux from day 15 to day 26 is also presented (right panel, control, n=6; *shSRSF6.0*, n=7, P=0.0479). **D,** Gene ontology analysis of the 342 overlapping transcripts in DMSO (vehicle) vs. P5091, $CD3^+$ T cells vs. T-ALL cells, as well as control vs. *shSRSF6.0* conditions.

Supplementary Figure 11. Zhou et al., 2019

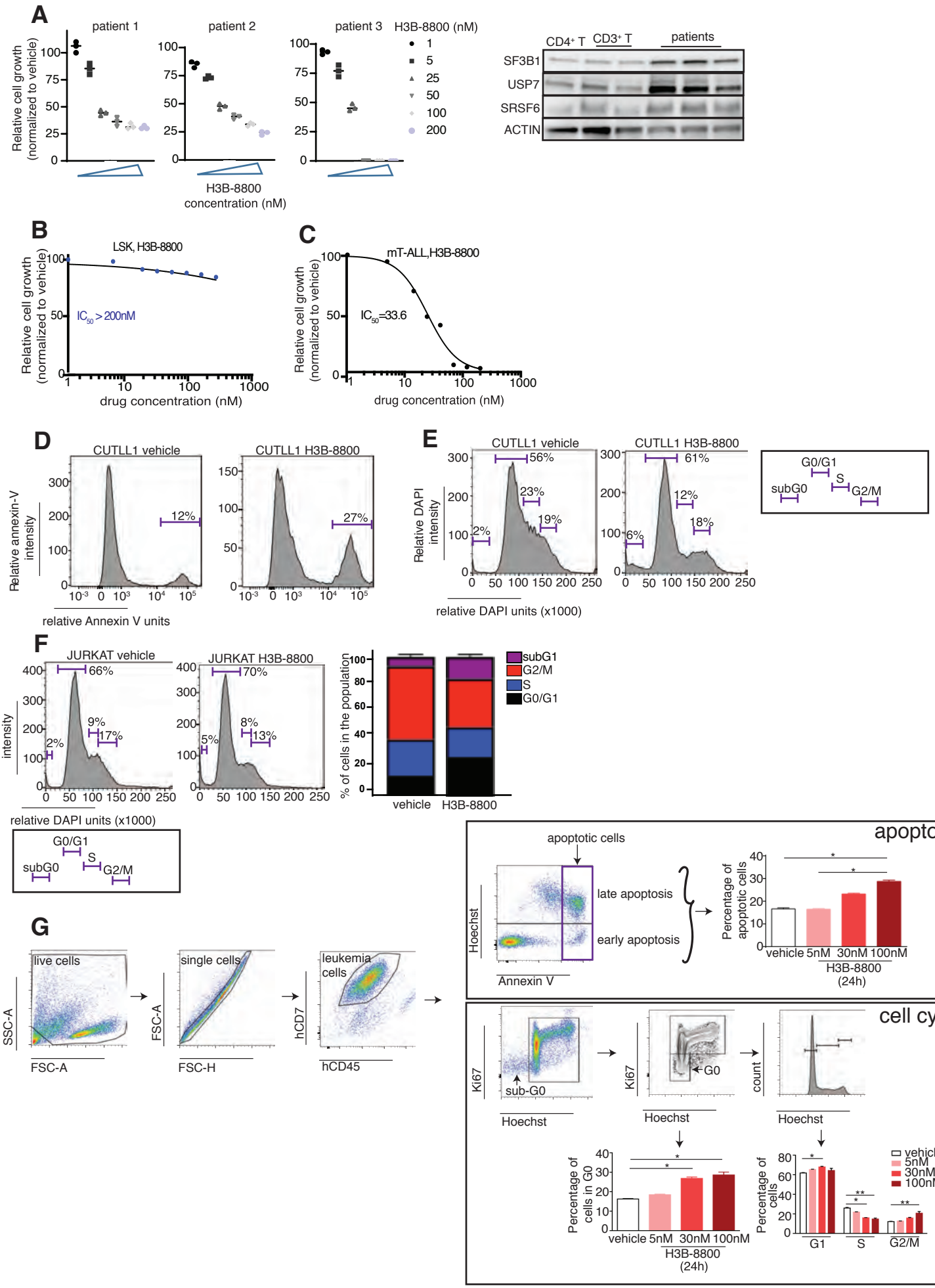

Supplementary Fig. 11. Splicing inhibition induces apoptotic cell death and blocks proliferation of T-ALL cells. A, Cell growth analysis of three patient samples using MTT assay upon splicing inhibition with increasing concentrations of H3B-8800 (up to 200nM) over a period of 48 h (left panel). Proteins levels of SRSF6 and USP7 in the patient samples treated and comparison to normal T cell samples is also shown (right panel). **B, C,** IC_{50} curves upon treatment of mouse LSK progenitor cells (**B**) or mouse T-ALL cells (720, **C**) with H3B-8800 over a period of 72 h. **D,** Annexin V staining of CUTLL1 cells for apoptosis upon treatment with 30nM H3B-8800 over a period of 48h. **E,** DAPI staining for the assessment of cell cycle changes upon treatment of CUTLL1 cells using 30nM H3B-8800 over a period of 48 h. **F,** DAPI staining for the assessment of cell cycle changes upon treatment of JURKAT cells using 30nM H3B-8800 over a period of 48 h. A representative biological replicate (left and middle panels) and average values of three biological replicates (right panel) are shown. Vehicle (DMSO) was used as the control. **G,** Gating strategy and related data points for isolation of live cells, single cells and human leukemia cells (M106), coupled to subsequent apoptosis and cell cycle analysis using a combination of Hoechst and Annexin V staining as well as Hoechst and Ki67 staining scheme correspondingly. Bar-graphs (left-most panels) represent apoptosis and cell cycle data for M106 samples over a period of treatment of 24h using 5 nM, 30nM and 100nM H3B-8800.

Supplementary Figure 12. Zhou et al., 2019

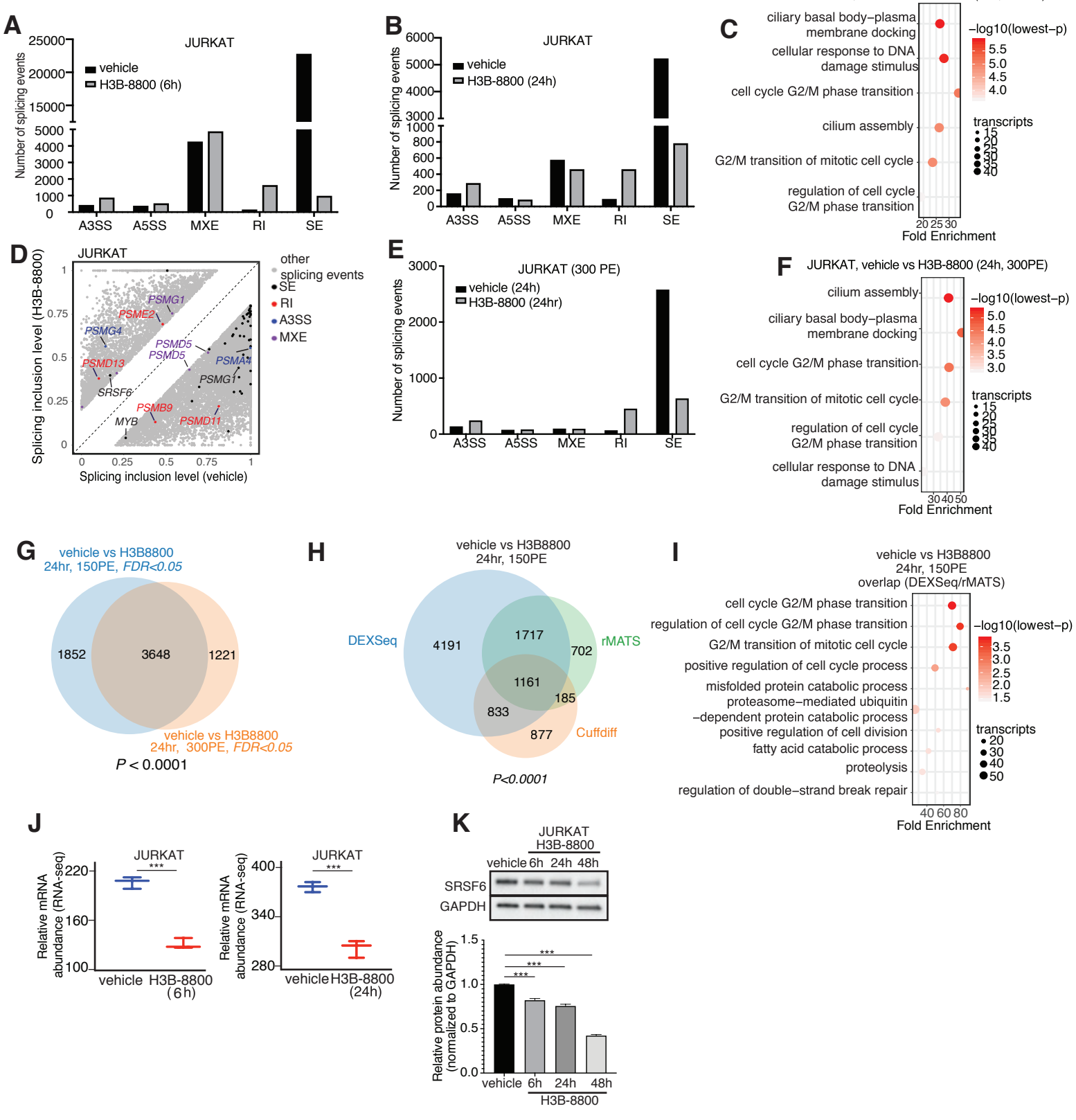

Supplementary Fig. 12. Inhibition of the splicing machinery affects the splicing pattern of a common set of leukemia-related genes. A, Representation of splicing events in JURKAT cells upon treatment with H3B-8800 or vehicle (DMSO) for 6 h, as identified via 150-read paired-end Illumina sequencing. Skipped exon (SE) was the main event category affected. **B,** Representation of splicing events in JURKAT cells upon treatment with H3B-8800 or vehicle (DMSO) for 24 h, as identified via 150-read paired-end Illumina sequencing. Skipped exon (SE) was the main event category affected. **C,** Gene ontology analysis of alternatively spliced transcripts in JURKAT cells upon treatment with H3B-8800 or vehicle (DMSO) for 24 h, as identified via 150-read paired-end Illumina sequencing. **D,** Scatterplot of splicing changes and distribution in H3B-8800-treated JURKAT cells (24h) compared to vehicle-treated JURKAT cells. Selected transcripts are colored by the type of differentially spliced event. Splicing is quantified using a "percent spliced in" value (PSI, or ψ value) and changes affecting at least 20% of transcripts are presented. **E,** Representation of splicing events in JURKAT cells upon treatment with H3B-800 or vehicle (DMSO) for 24 h, identified via 300 paired-end Illumina sequencing. Similarly to panel B, skipped exon (SE) was the main event category affected. **F,** Gene ontology analysis of alternatively spliced transcripts in JURKAT cells upon treatment with H3B-8800 or vehicle (DMSO) for 24 h, as identified via 300-read paired-end Illumina sequencing. **G.** Overlap of transcripts presenting with splicing changes in JURKAT cells upon treatment with H3B-8800 or vehicle (DMSO) for 24h, as identified via 150-read and 300-read paired-end sequencing. Analysis shows 3648 transcripts common between the two sequencing comparisons ($P<0.001$). **H,** Overlap between transcripts with differentially spliced events from the rMATS analysis, transcripts with differentially used exons from the DEXSeq analysis and isoform changes from Cufflink (Cuffdiff) analysis in H3B-8800- vs vehicle (DMSO)-treated JURKAT cells (24h, 150 PE Illumina sequencing). **I,** Gene ontology analysis using overlapping genes from H. **J,** Assessment of SRSF6 mRNA levels using RNA-sequencing upon treatment of JURKAT cells with H3B-8800 over a period of 6h and 24h (***, $P<0.001$). **K,** Assessment of SRSF6 protein levels upon treatment of JURKAT cells with H3B-8800 over a period of 6h, 24h or 48h. Immunoblot (top panel) and band intensity quantification from three independent studies (bottom panel) are shown (***, $P<0.001$).

Supplementary Figure 13. Zhou et al., 2019

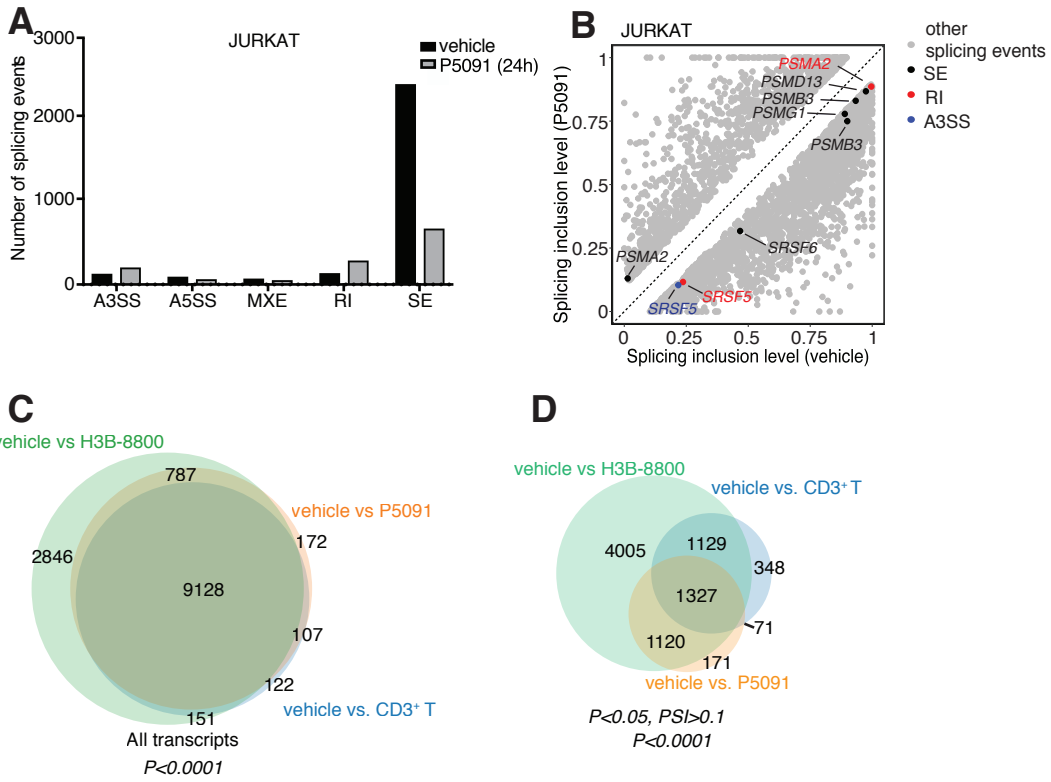

Supplementary Fig. 13. Inhibition of USP7 affects the splicing pattern of a common set of leukemia-related transcripts, highly overlapping with H3B-8000-affected transcripts. A, Representation of splicing events in JURKAT cells upon treatment with P5091 or vehicle (DMSO) for 24 h. Skipped exons (SE) were the main event category affected. **B,** Scatterplot of splicing changes and distribution in P5091-treated JURKAT cells (24h) compared to vehicle-treated JURKAT cells. Selected transcripts are colored by the type of differentially spliced event. Splicing is quantified using a "percent spliced in" value (PSI, or ψ value) and changes affecting at least 10% of transcripts are presented. **C, D,** Overlap of transcripts differentially spliced in vehicle-treated T-ALL cells compared to H3B-8800- and P5091-treated T-ALL cells as well as $CD3^+$ T cells for all transcripts **(C**) and for transcripts presenting with at least 10% splicing changes (**D**, $P<0.05$; $PSI>0.10$). **E,** Gene ontology analysis for the overlapping transcripts from panel **D. F,** Sashimi plots representing splicing and exon-exon junctions for the *PSMG1* transcript in JURKAT cells treated with H3B-8800 for 6 h. **G,** Sashimi plots representing splicing and exon-exon junctions for the *PSMG1* transcript in JURKAT cells treated with P5091 for 24 h. In both **F, G,** RNA sequence is shown along the horizontal axis. Purple rectangle highlights exon 4. Thicker sections represent exons coding for protein sequence. Numbers over the lines connecting exons represent the number of reads mapped to that junction.

Supplementary Figure 14. Zhou et al., 2019

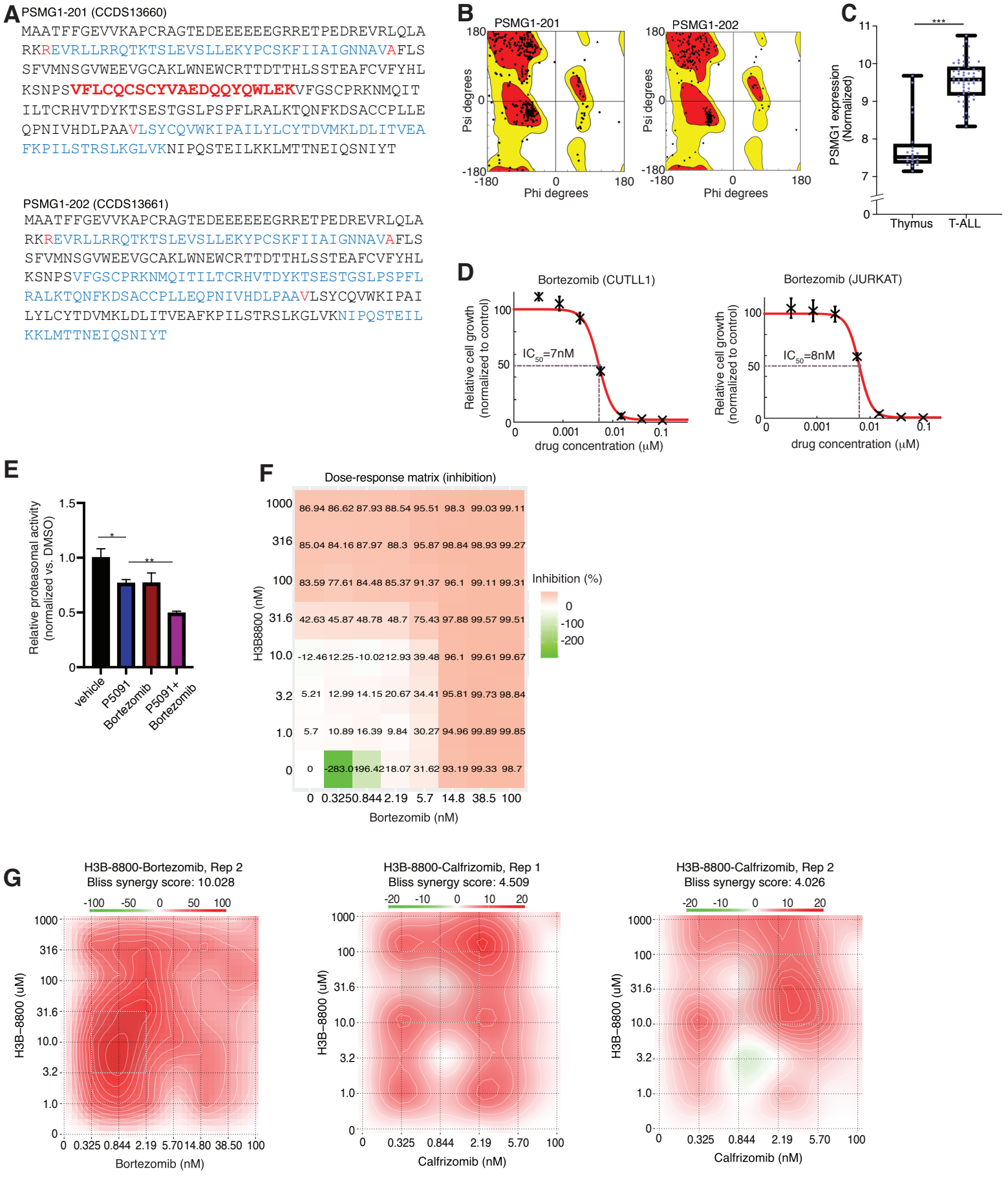

Supplementary Fig. 14. Splicing and proteasomal inhibition act synergistically to block T-ALL growth. A, Sequences for *PSMG1-201* and *PSMG1-202*-encoded proteins. Sequence of *201*-encoded protein that is missing from *202* is colored red. Sequences corresponding to exons are labelled as black and blue. **B,** Probabilistic modeling for amino acid positioning. Amino acids are represented by the black dots. Red denotes high probability for the amino acid position, yellow denotes medium probability and white denotes low probability. Note that our model can predict fairly well the amino acid position for both 201 and 202. **C,** PSMG1 expression in T-ALL versus thymocytes. 57 T-ALL patient samples and 21 thymocytes were used in this comparison, as in **Supplementary Fig. 7C, D.** (***, $P<0.001$). **D,** IC_{50} curves upon treatment of CUTLL1 (left panel) and JURKAT (right panel) cells with bortezomib over a period of 72 h. **E,** Measurement of proteasome activity using a luminescence-based method upon treatment of JURKAT cells with 10mM P5091 for 24h, 0.5nM bortezomib (4h treatment) or their combination (*, $P<0.05$, **, $P<0.01$). **F,** Dose-response matrix (demonstrating inhibition) for the proteasomal inhibitor bortezomib as well as H3B-8800 over a period of 3 days in JURKAT cells. Green represents low inhibition/higher cell growth and red represents drug cytotoxicity/lower cell growth. **G,** Synergy heatmaps for treatment with H3B-8800 and the proteasomal inhibitors bortezomib (left panel) and carfilzomib (middle and right panels) over a period of 3 days in JURKAT cells. Red color denotes drug synergy. Note there are extensive areas of drug synergy in a wide range of concentrations. The H3B-8800-Bortezomib combination presents with higher synergy than the H3B-8800-Calfrizomib combination.

Supplementary Figure 15. Zhou et al., 2019

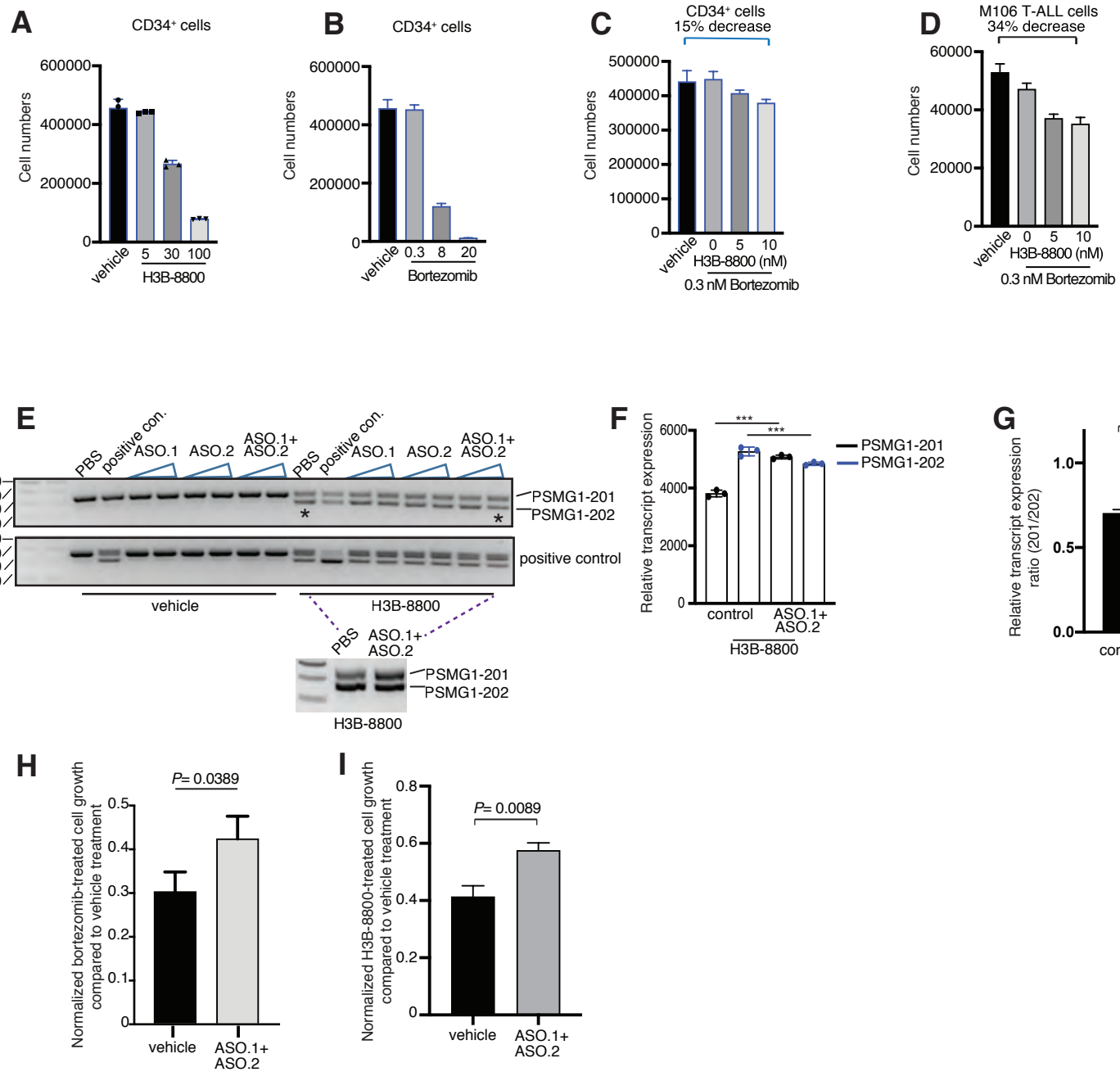

Supplementary Fig. 15. Toxicity analysis for splicing inhibition. A-C, Cell growth for CD34+ cells upon treatment with H3B-8800 (**A**), bortezomib (**B**), and their combination (**C,** *n=3*). **D,** Cell growth of M106 T-ALL patient sample, upon treatment with combination of H3B-8800 and bortezomib. Three technical replicates from one representative biological experiment is shown (*n=2* biological replicates). **E,** PCR-based analysis coupled to electrophoresis for detection of PSMG1-201 and PSMG-202 isoforms upon transfection of CUTLL1 cells with antisense oligos (ASOs) blocking PSMG1 exon 4 skipping and treatment with vehicle or H3B-8800 (30nM, 6h). **F,** Quantification of band intensities presented in **E** (*n=3,* ***, *P*<0.001)). **G,** Relative expression rate of 202 transcript compared to 201 transcript (*n=3*, **, *P*=0.0043). **H, I,** Relative growth of bortezomib (10nM)- (**H**) and H3B-8800 (30nM)-treated (**I**) cells compared to vehicle (DMSO)-treated cells is shown for *PBS*- and *ASO1+ASO2*-treated CUTLL1 cell populations, over a period of 72h of drug treatment. Cells were transfected with PBS or the oligos 24h before initiation of drug treatment. The NADPH-based MTT assay was used to measure cell growth. *ASO1+ASO2*-treated CUTLL1 cells present with a decreased sensitivity to splicing inhibition compared to control cells (*n=3*).